Radio Science, Volume 11, Number 10, pages 833-845, October 1976

A comparative study of three techniques for using the spectral matrix in wave analysis

C. W. Arthur,[1] *R. L. McPherron,*[1] *and J. D. Means*

Institute of Geophysics and Planetary Physics, University of California, Los Angeles, California 90024

(Received November 7, 1975.)

Digital power spectral analysis and coherency analysis are powerful techniques for studying ultra-low-frequency (ULF) waves in the earth's magnetosphere. Wave polarization parameters provided by these techniques are important in the development of theoretical models for wave generation. Because of this, it is important to understand the capabilities of the digital analysis techniques. Three different techniques of using the spectral matrix to do wave analysis have been presented in the literature. Because data for wave studies involve measurement in arbitrary coordinate systems, it is necessary to transform the spectral matrix to the principal plane of the wave before coherency analysis can be performed. The fundamental differences in the three techniques lie in how they determine the transformation to the principal plane. A comparative study of these three techniques was done using simulated data involving known wave and noise properties and real ULF wave event data from the geosynchronous satellites ATS 1 and ATS 6. In general, the quality of performance of the three different techniques on both simulated and real wave events was approximately the same.

INTRODUCTION

Naturally-occurring ultra-low-frequency (ULF) waves (or magnetic pulsations) in the earth's magnetosphere have been studied extensively for many years. However, because of the low frequencies involved (1 to 1000 mHz), traditional analog techniques have had only limited usefulness. The increasing availability of digital data, on the other hand, allows the use of digital power spectral analysis and coherency analysis, powerful techniques for the analysis of ULF waves. The knowledge of the wave polarization parameters provided by these techniques is important in the development of theoretical models of wave generation. Thus, because of the importance of these parameters, it is necessary to have an understanding of the capabilities and limitations of the digital analysis techniques which are being used.

Using techniques presented by *Born and Wolf* [1964] based on the principles of statistical optics as applied to quasi-monochromatic wave theory, *Fowler et al.* [1967] developed a technique for determining the polarization parameters (percent polarization, ellipticity, and azimuth) from the spectral matrix for a plane wave in two dimensions. However, data for ULF wave studies usually involve measurements in a three-dimensional coordinate system oriented arbitrarily with respect to the waves. Three different techniques have been presented in the literature [*McPherron, et al.*, 1972; *Means*, 1972; *Samson*, 1973] dealing with the three-dimensional situation. These three techniques, while mathematically dissimilar, are all based on the assumption that, at any single frequency, a single plane wave, propagating along the normal to the plane, is present. Thus, these techniques should not be used for analysis of nonplanar waves unless planarity is reasonably approximated. In the case of multiple waves with the same frequency, the parameters determined by the analysis represent the average of the parameters for the individual waves. For waves with strongly dissimilar characteristics but the same frequency (a fairly rare event in nature), these results will be anomalous. Indications that this situation has occurred can be obtained from the percent polarization and the relative size of the eigenvalues. For multiple waves with only slightly dissimilar characteristics, there will be no way to identify the presence of the multiple waves, but the character of the waves determined by the analysis will be essentially correct.

In this paper, we briefly present the details of

[1] Also Department of Geophysics and Space Physics.

these three techniques and report the results of a comparative study of the techniques made using both simulated data and real ULF wave data from the geosynchronous satellites ATS 1 and ATS 6. The purpose of this paper is twofold: first, to present as succinctly as possible the pertinent mathematics of these three techniques in order to facilitate their use by other researchers, and second, to delineate the capabilities and limitations of the different techniques and discuss which is best for certain types of application. Particular importance is given to the criteria appropriate for application to studies involving large numbers of events and requiring the calculation of hundreds of power spectra and their associated polarization parameters. No effort is made to determine whether any of these techniques represents an absolute best in terms of signal detection theory. Rather, the conclusions of the study bear on which of the three techniques presently in the literature is the best for certain applications.

DESCRIPTION OF THE TECHNIQUES

Power spectral analysis. The determination of the 3 × 3 spectral matrix in the measurement coordinate system is the first step in the wave analysis procedure. This matrix has elements which consist of all possible cross spectra between pairs of components. One such matrix is determined for each frequency estimate. The analysis described below is done for each frequency estimate. Several techniques are available for determination of the spectral matrix (such as those requiring use of the Fast Fourier Transform or the maximum entropy method), but they are not discussed here.

Coherency analysis. Once the spectral matrix has been rotated into the principal axis system by one of the techniques described below, the polarization parameters described by *Born and Wolf* [1964] and *Fowler et al.* [1967] can be determined. If only two components of the field are measured, this coherency analysis can be done in that plane, but the results may be misleading if the measurement plane is not close to the principal plane of the wave.

The spectral matrix in the principal plane of a wave has the form

$$\mathbf{J} = \begin{bmatrix} J_{xx} & J_{xy} \\ J^*_{xy} & J_{yy} \end{bmatrix} \tag{1}$$

where J_{xx} and J_{yy} are real and J_{xy} is imaginary if the major axis of the wave is oriented along the X or Y axis, complex if it is not. The percent polarization (% Pol) is determined from the ratio of coherent power to total power in the plane and can be calculated from

$$\%\ \text{Pol} = 100\,[1 - 4 \det \mathbf{J}/(\text{Tr}\,\mathbf{J})^2]^{1/2} \tag{2}$$

Ellipticity (El) is defined as the ratio of the minor to major axis of the polarization ellipse of the wave and is given by

$$\text{El} = \tan \beta \tag{3}$$

where β is determined from

$$\sin 2\beta = \frac{2\ \text{Im}\ J_{xy}}{[(\text{Tr}\,\mathbf{J})^2 - 4 \det \mathbf{J}]^{1/2}} \tag{4}$$

Azimuth (ϕ), the angle the major axis makes with the X axis, is defined by

$$\tan 2\phi = 2\,(\text{Re}\ J_{xy})/(J_{xx} - J_{yy}) \tag{5}$$

For a plane wave in the principal axis system

$$\begin{aligned} x(t) &= a \exp[i(\omega t)] \\ y(t) &= b \exp[i(\omega t - \pi/2)] \\ z(t) &= 0 \end{aligned} \tag{6}$$

the spectral matrix at the frequency ω is given by

$$\mathbf{J} = \begin{bmatrix} a^2 & iab & 0 \\ -iab & b^2 & 0 \\ 0 & 0 & 0 \end{bmatrix} \tag{7}$$

and the upper left 2 × 2 submatrix corresponds to the matrix in (1).

Wave analysis. The coherency analysis described above is most valid when performed in the principal plane of a wave. However, most wave measurements are usually made in a coordinate system oriented arbitrarily with respect to the principal axis system. Therefore it is necessary to determine a rotation matrix with which to transform the spectral matrix into this principal axis system. The three techniques of wave analysis compared in this paper are, in effect, three different ways to determine this rotation matrix. There are also some subtle differences between the techniques which are beyond the scope of this paper.

Technique 1 [*McPherron, et al.*, 1972] is based on diagonalization of the real part of the spectral

matrix. Let **G** be the spectral matrix in the measurement system. The real part of **G** (Re **G**) is then diagonalized using standard eigenanalysis procedures. If we assume that the direction of minimum variance corresponds to the direction of wave propagation (as indicated by (6) and (7)), then the matrix of eigenvectors (**T**) can be used to transform the entire spectral matrix into the principal axis system

$$\mathbf{G}' = \mathbf{T}^T \mathbf{G}\, \mathbf{T} \tag{8}$$

The diagonal elements of **G**′ are the eigenvalues of **G** and correspond to the autospectra of the three principal axis coordinates. The upper left 2 × 2 submatrix of **G**′, i.e.,

$$\begin{bmatrix} G'_{11} & G'_{12} \\ G'^{*}_{12} & G'_{22} \end{bmatrix}$$

can now be subjected to the coherency analysis described above to determine the percent polarization and ellipticity. Since the X axis is required by the eigenanalysis to lie along the direction of maximum variance, the azimuth determined from (5) will always be zero for this technique. The orientation of the major axis (X) and the direction of propagation (Z) relative to the input coordinate system can be determined from the matrix **T** by means of

$$\tan\theta_x = (T_{11}^2 + T_{21}^2)^{1/2}/T_{31} \tag{9}$$

$$\tan\phi_x = T_{21}/T_{11} \tag{10}$$

$$\tan\theta_z = (T_{13}^2 + T_{23}^2)^{1/2}/T_{33} \tag{11}$$

$$\tan\phi_z = T_{23}/T_{13} \tag{12}$$

Technique 2 [*Means*, 1972] obtains the components of the unit wave normal vector ($\hat{k}$) directly from the imaginary part of the spectral (or covariance) matrix:

$$\mathrm{Im}\,\mathbf{G} = \begin{bmatrix} 0 & \mathrm{Im}\,G_{xy} & \mathrm{Im}\,G_{xz} \\ -\mathrm{Im}\,G_{xy} & 0 & \mathrm{Im}\,G_{yz} \\ -\mathrm{Im}\,G_{xz} & -\mathrm{Im}\,G_{yz} & 0 \end{bmatrix} \tag{13}$$

If we define a variable p such that

$$p = [(\mathrm{Im}\,G_{xy})^2 + (\mathrm{Im}\,G_{xz})^2 + (\mathrm{Im}\,G_{yz})^2]^{1/2} \tag{14}$$

then the components of $\hat{k}$ are given by

$$k_x = \mathrm{Im}\,G_{yz}/p \tag{15}$$

$$k_y = \mathrm{Im}\,G_{xz}/p \tag{16}$$

$$k_z = \mathrm{Im}\,G_{xy}/p \tag{17}$$

The above is true for a right-hand polarized wave; for a left-handed wave, $\hat{k}' = -\hat{k}$ must be used.

The spectral matrix is then rotated into a new coordinate system in which $\hat{k}$ is along the Z axis. Although the particular choice of the X-Y axis is arbitrary, it is convenient to have the X axis coplanar with $\hat{k}$ and $\hat{B}$ (where $\hat{B}$ represents the magnetic field direction) and Y perpendicular to this plane. If this rotation is accomplished by the matrix $\mathbf{T}_1$, then

$$\mathbf{G}' = \mathbf{T}_1^T \mathbf{G}\, \mathbf{T}_1 \tag{18}$$

In this system, the major axis of the polarization ellipse is not necessarily aligned with the X coordinate axis. Coherency analysis is performed on the upper left 2 × 2 submatrix of **G**′. Using the azimuth angle ϕ determined by this coherency analysis, another rotation is defined that completes the transformation of **G** into the principal axis system, so that the X axis is aligned with the major polarization axis

$$\mathbf{G}'' = \mathbf{T}_2\, \mathbf{G}'\, \mathbf{T}_2^T \tag{19}$$

where

$$T_2 = \begin{bmatrix} \cos\phi & \sin\phi & 0 \\ -\sin\phi & \cos\phi & 0 \\ 0 & 0 & 1 \end{bmatrix} \tag{20}$$

But substituting from (18) for **G**′ in (19), we have

$$\mathbf{G}'' = \mathbf{T}_2\, \mathbf{T}_1^T \mathbf{G}\, \mathbf{T}_1\, \mathbf{T}_2^T, \quad \mathbf{G}'' = (\mathbf{T}_1\, \mathbf{T}_2^T)^T \mathbf{G}\, (\mathbf{T}_1\, \mathbf{T}_2^T) \tag{21}$$

So by comparison with (8), we see that $\mathbf{T}_1\, \mathbf{T}_2^T$ gives a transformation equivalent to **T**, and the orientation angles of the X and Z axes relative to the input system can be determined from $\mathbf{T}_1\, \mathbf{T}_2^T$ in the same way as from **T**, (9)–(12).

The above analysis procedure is invalid for a linearly polarized plane wave, which has a purely real spectral matrix. However, the direction of the linear axis can be determined as follows

$$L_x = [G_{xx}/(\mathrm{Tr}\,\mathbf{G})^2]^{1/2} \tag{22}$$

$$L_y = G_{xy}/(\mathrm{Tr}\,\mathbf{G})L_x \tag{23}$$

$$L_z = G_{xz}/(\mathrm{Tr}\,\mathbf{G})L_x \tag{24}$$

Once $\hat{L}$ has been determined, it can be used in

the same way as $\hat{k}$ to define the appropriate rotations. However, $\hat{L}$ should be used to define the X, rather than the Z axis.

Technique 3 [*Samson*, 1973] uses the fact that several different expansions of the spectral matrix are possible. The most useful analytically is expansion as a series of nondisjoint idempotent matrices. Although *Samson* [1973] develops the expressions in the general n-dimensional case with two- and three-dimensional examples, only the three-dimensional expressions (Samson's equations 32, 33) are appropriate to our study and are presented here.

The first step in the technique is the determination of the eigenvalues and eigenvectors of the entire Hermitian spectral matrix **G**. The diagonalization of a complex matrix is a difficult computational problem. It was accomplished in our study through the use of a package of algorithms developed at the Argonne National Laboratory and given the acronym EISPACK [*Smith et al.*, 1974]. (The FORTRAN coding necessary for this computation is presented in this reference.)

For the spectral matrix **G**, if **U** is the unitary matrix of eigenvectors and $\lambda_1 \geq \lambda_2 \geq \lambda_3$ are the eigenvalues, it can be shown that the following expansion holds:

$$\mathbf{U}^{\dagger}\mathbf{G}\mathbf{U} = \lambda_3 \begin{bmatrix} 1 & 0 & 0 \\ 0 & 1 & 0 \\ 0 & 0 & 1 \end{bmatrix} + (\lambda_2 - \lambda_3) \begin{bmatrix} 1 & 0 & 0 \\ 0 & 1 & 0 \\ 0 & 0 & 0 \end{bmatrix} + (\lambda_1 - \lambda_2) \begin{bmatrix} 1 & 0 & 0 \\ 0 & 0 & 0 \\ 0 & 0 & 0 \end{bmatrix} \tag{25}$$

Equation (25) represents an expansion in terms of three uncorrelated stochastic processes which, in order from left to right, are unpolarized, partially polarized, and purely polarized. *Samson* [1973] then defined some parameters which are not available from the other techniques. Noting that the total power is, as usual, given by $(\lambda_1 + \lambda_2 + \lambda_3)$, the relative power present in each of these processes (or polarization states) is

$$R_1 = \frac{\lambda_1 - \lambda_2}{\lambda_1 + \lambda_2 + \lambda_3} \quad \text{purely polarized} \tag{26}$$

$$R_2 = \frac{2(\lambda_2 - \lambda_3)}{\lambda_1 + \lambda_2 + \lambda_3} \quad \text{partially polarized} \tag{27}$$

$$R_3 = \frac{3\lambda_3}{\lambda_1 + \lambda_2 + \lambda_3} \quad \text{unpolarized} \tag{28}$$

The three-dimensional degree of polarization, P, is given by (Samson's equation 32):

$$P^2 = (1/2)[(\lambda_1 - \lambda_2)^2 + (\lambda_1 - \lambda_3)^2 + (\lambda_2 - \lambda_3)^2] \div (\lambda_1 + \lambda_2 + \lambda_3)^2 \tag{29}$$

Note that P is significantly different from the percent polarization (2).

The idempotent matrix $\mathbf{D}_1$, which corresponds to the purely polarized state is given by

$$\mathbf{D}_1 = \mathbf{U} \begin{bmatrix} 1 & 0 & 0 \\ 0 & 0 & 0 \\ 0 & 0 & 0 \end{bmatrix} \mathbf{U}^{\dagger} \tag{30}$$

Similar definitions hold for $\mathbf{D}_2$ and $\mathbf{D}_3$, corresponding to the other two states, but they are not used in this study. Because **U** is complex, $\mathbf{D}_1$ is

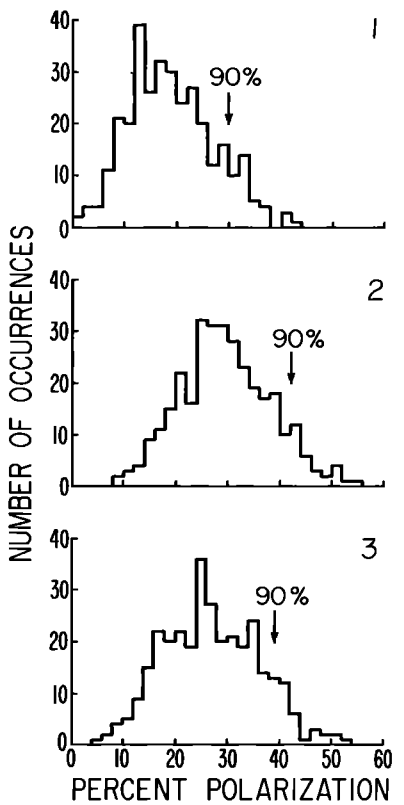

Fig. 1. Distributions of percent polarization determined by the three techniques for signals composed of gaussian random noise.

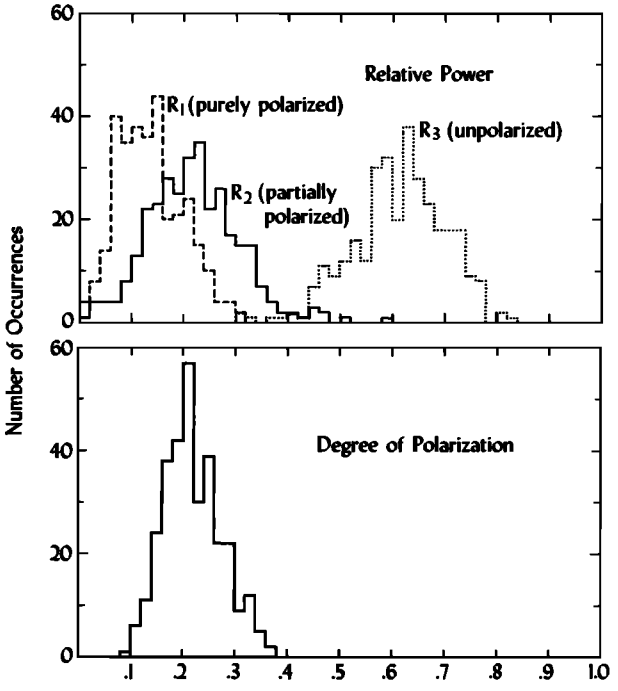

Fig. 2. Distributions of the polarization parameters of the Samson method (technique 3) for signals composed of gaussian random noise.

difficult to interpret directly. As stated by Samson, diagonalization of the real part of $\mathbf{D}_1$, which can be accomplished by using either technique 1 or 2, simplifies its interpretation and allows us to calculate the parameters we are using for comparison. We chose to use technique 2 to find $\mathbf{T}_a$ such that

$$\mathbf{T}_a^T \mathbf{D}_1 \mathbf{T}_a = \mathbf{J} \tag{31}$$

where Re $\mathbf{J}$ is diagonal. The ellipticity of the wave can then be determined from coherency analysis of the upper left 2 × 2 submatrix of $\mathbf{J}$ (31). At this point, we must extend the technique proposed by Samson so that we can calculate the other physical parameters we are using in our study. The matrix $\mathbf{T}_a$ corresponds to $\mathbf{T}$ in (8) and the orientation angles can be determined as before, (9)-(12). The azimuth should be zero. The percent polarization calculated from this $\mathbf{J}$ (31) is not meaningful since only polarized power is included in $\mathbf{D}_1$. Instead, $\mathbf{T}_a$ is used to transform $\mathbf{G}$:

$$\mathbf{S} = \mathbf{T}_a^T \mathbf{G} \mathbf{T}_a \tag{32}$$

The upper left 2 × 2 submatrix of $\mathbf{S}$ can now be used to determine the percent polarization. The diagonal elements of $\mathbf{S}$ are equivalent in meaning to those of $\mathbf{G}'$ in (8) and $\mathbf{G}''$ in (19).

COMPARISON OF THE TECHNIQUES

Noise response. In order to study the noise response of the three techniques, several events composed of three independent components of gaussian random noise were generated and analyzed. It is particularly important to know what levels of percent polarization are calculated when only noise is present. This knowledge allows us to establish a cutoff level for use in deciding whether a polarized wave is present in the signal, or whether the wave signal is sufficiently unaffected by noise for the other calculations of its properties to be meaningful. Distributions of the percent polarization values determined for the gaussian random noise are shown in Figure 1. The arrows mark the value below which 90% of the distribution falls. For technique 1, this value is 30%; for technique

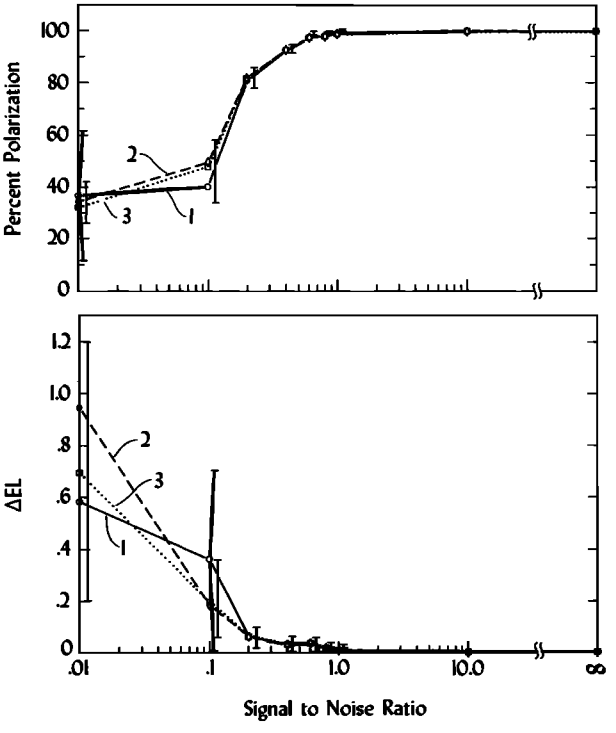

Fig. 3. Quality of computer-determined polarization parameters: percent polarization and ΔEL. Circles and solid lines indicate results for technique 1; diamonds and dashed lines for technique 2; squares and dotted lines for technique 3. Error bars are discussed in the text.

2, 42%; and for technique 3, 39%. Thus, when using these techniques for wave analysis, calculated wave properties should be suspect if the percent polarization is lower than the values stated above. It should be mentioned, however, that the value for technique 3 is not entirely independent of that for technique 2. If technique 1 had been used to diagonalize $\mathbf{D}_1$ in technique 3, its 90% value might have been lower.

For technique 3, the behavior of the other parameters defined by *Samson* [1973] is also important. The distributions of these parameters (see equations 26 through 29) for gaussian random noise are shown in Figure 2. Values of $R_1 > 0.3$ and $P > 0.35$ would seem to be adequate to imply the presence of a polarized wave. These values, however, depend strongly on the number of degrees of freedom used in the spectral analysis. In our analysis, 26 degrees of freedom were used. *Samson* [1973], however, uses only 7 degrees of freedom and finds that $R_1 > 0.6$ and $P > 0.7$ should be used as criteria. Thus, it is important to determine which threshold values of R_1 and P are appropriate for the number of degrees of freedom used in a particular study.

Simulated wave events. Four types of simulated wave events were studied. The events were generated with known values of the polarization parameters (ellipticity, orientation angles). Independent gaussian random noise was added to each axis. Nine different values of amplitude signal-to-noise ratio (snr) were used for each event. These values were ∞, 10.0, 1.0, 0.8, 0.6, 0.4, 0.2, 0.1, and 0.01.

The first type of event studied was simply a single elliptical plane wave with known period and ellipticity, and known but arbitrary orientation. Five such events, each done for the nine snr values, were generated and analyzed. In each case, the peak of the spectrum was exactly on the known input frequency. The values of all the polarization parameters at the peak of each spectrum were determined.

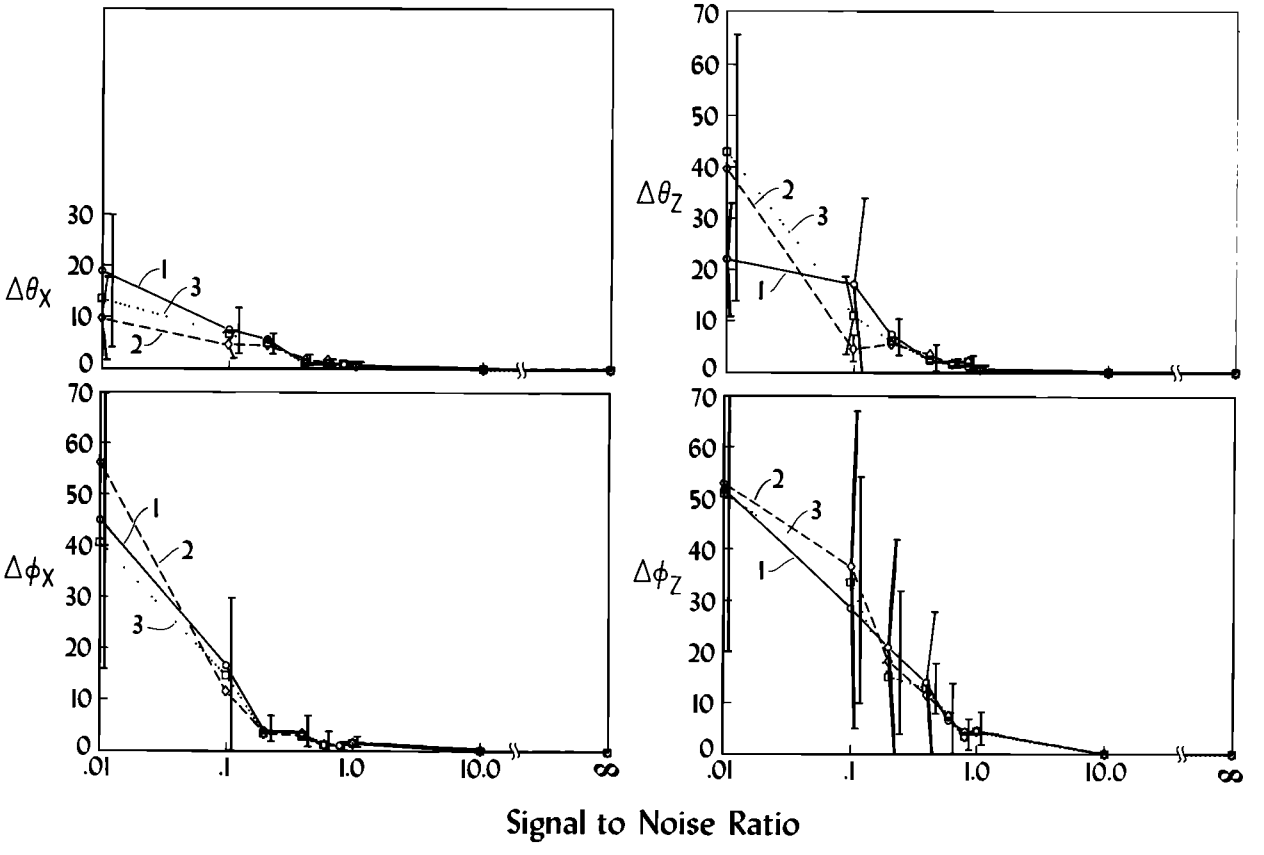

Fig. 4. Quality of computer-determined polarization parameters: $\Delta\theta_x$, $\Delta\phi_x$, $\Delta\theta_z$, and $\Delta\phi_z$. Symbols are the same as in Figure 3.

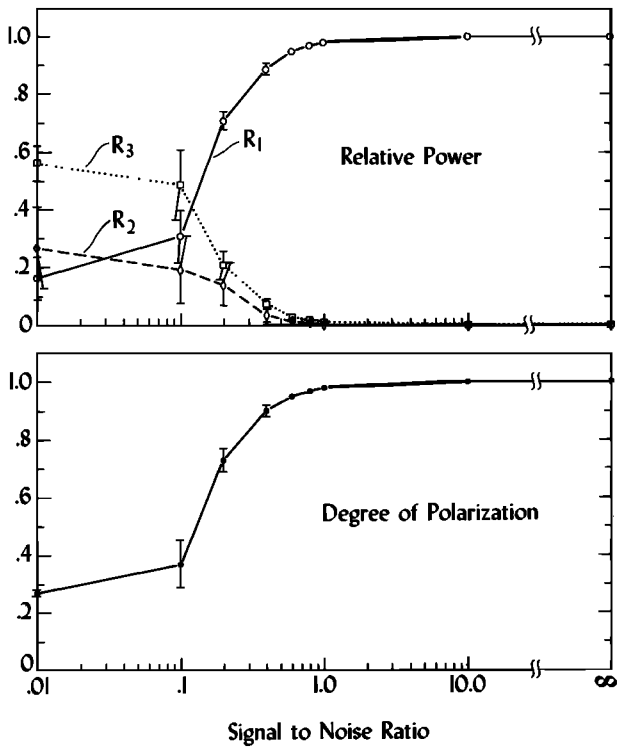

Fig. 5. Variation of polarization parameters of the *Samson* [1973] method (technique 3) with snr.

The differences between the calculated input values of ellipticity, θ_x, ϕ_x, θ_z, ϕ_z were calculated for each event and are referred to as ΔEL, $\Delta\theta_x$, $\Delta\phi_x$, $\Delta\theta_z$, and $\Delta\phi_z$. The mean differences for the five events were then calculated. Figure 3 shows the mean values of the calculated percent polarization and ΔEL plotted as a function of snr for each technique. Figure 4 shows the results for $\Delta\theta_x$, $\Delta\phi_x$, $\Delta\theta_z$, and $\Delta\phi_z$. In both figures the error bars plotted just to the right of the points show a representative standard error in the mean. If the standard error for one technique was significantly different from that for the others, it was plotted attached to its appropriate point. It is clear from both figures that all three techniques give excellent results for snr's ≥ 0.2. A similar result is clear in the extra parameters of technique 3. The mean and standard error in the mean for these four parameters are shown in Figure 5. For snr's < 0.2, $R_1 < 0.3$, R_3 is high, and $P < 0.4$, all of which indicate that the dominant signal is the noise.

Two events in which one noise component was of larger amplitude than the other two were generated and analyzed. The axis nearest the direction of wave propagation had the largest noise; the noise in the other two axes was only 70% as large. This approximates the ATS 1 situation for transverse waves. The results for all three techniques were still quite acceptable for snr's > 0.2.

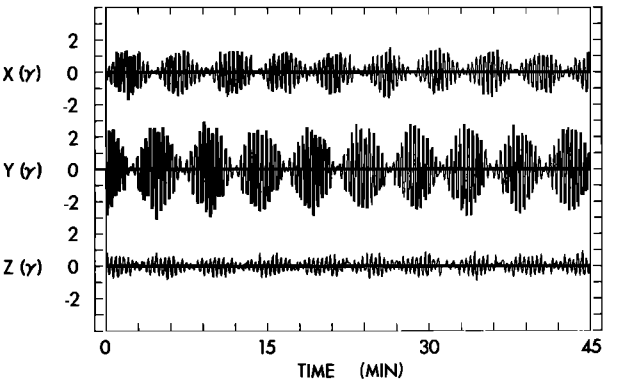

Fig. 6. Waveform of a portion of a simulated wave event composed of two plane waves with different periods, ellipticities, and orientations. The snr is 2.0.

Eight events having various ellipticities less than 0.1, all with snr's of 1.0, were analyzed to compare the performances of the three techniques on linear waves. In this test, the linear expressions given in (22)–(24) for technique 2 (and thus also technique 3) were used only when the ellipticity was less than 0.01. For these very simple simulated wave events, all three techniques performed equally well at determining ellipticity and orientation of the major (or linear) axis.

The second type of wave studied had a time-varying direction of propagation. As before, an elliptical plane wave of known period, ellipticity, and orientation was used. The orientation angles were incremented every four wave periods. Two such events were studied: one in which the increment was small,

TABLE 1. Input parameters for the simulated wave event shown in Figure 6.

Digitization interval	5 sec	
Period	25 sec	23 sec
Ellipticity	0.5	−0.5
θ_x	80°	75°
ϕ_x	80°*	85°*
θ_z	15°	20°
ϕ_z	31.2°*	42.4°*

*$A \pm 180°$ ambiguity exists in the determination of these angles, i.e., $\phi \pm 180°$ is the same as ϕ.

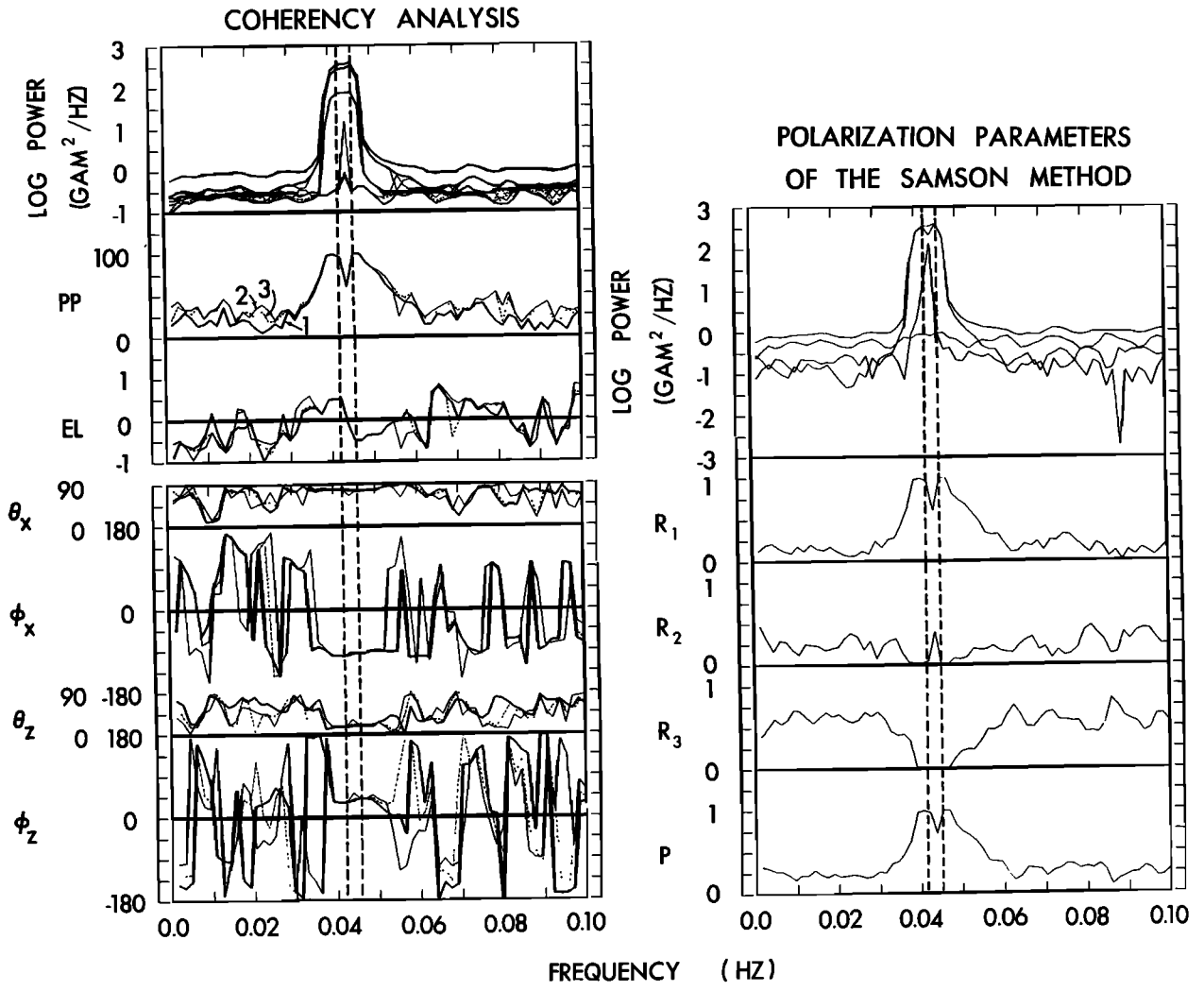

Fig. 7. Analysis results for the event illustrated in Figure 6. On the left-hand side of the figure, results for technique 1 are plotted with a heavy line; technique 2, light line; technique 3, dotted line. The upper panel on the left contains plots of the trace and x, y, and z autospectra in the principal axis system. In the top panel on the right, the trace and the power in each polarization state are plotted. The vertical dashed lines indicate the input wave periods.

and one in which it was large. In both cases, the orientation calculated by the analysis corresponded to an average of the orientations which occurred during the event. Good results were again obtained for snr's greater than 0.2.

The third type of wave event studied had two plane waves with different characteristics occurring simultaneously. The periods of the two waves were chosen so that they were separated by only one spectral estimate. The waveform of this simulated event is shown in Figure 6. The input parameters of the two waves are given in Table 1. The results

TABLE 2. Input parameters for the simulated wave event shown in Figure 8.

Digitization interval	5 sec	
Period	25 sec	23 sec
Ellipticity	0.5	0.4
θ_x	75°	80°
ϕ_x	70°*	80°*
θ_z	20°	15°
ϕ_z	27.4°*	31.2°*

*See note in Table 1.

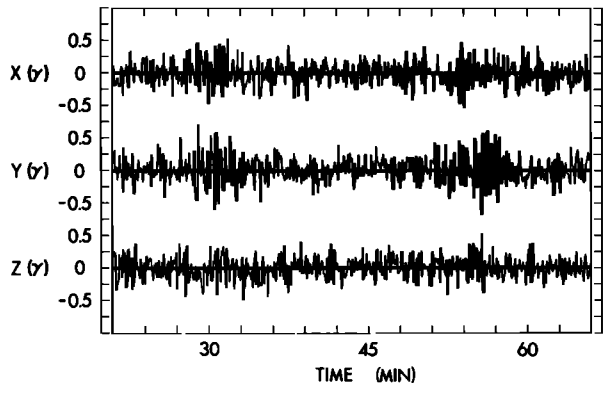

Fig. 8. Waveform of a portion of a simulated wave event composed of two wave bursts with gaussian amplitude envelopes and different periods, ellipticities, and orientations. The snr is 1.0.

of the analysis of this event using all three techniques are shown in Figure 7. The results obtained by the different techniques not only agree among themselves, but also agree quite well with the input parameters. In fact, all three techniques did an excellent job even for quite low snr's. The parameters of the *Samson* [1973] method (technique 3) also behaved as expected. Note the indication of a significant amount of partially polarized power in the spectral estimate separating the two input waves.

The final type of simulated wave event was composed of two nonsimultaneous wave bursts with gaussian amplitude envelopes and different characteristics. The input parameters for this event are given in Table 2, and a portion of the waveform for an snr of 1.0 is shown in Figure 8. This event

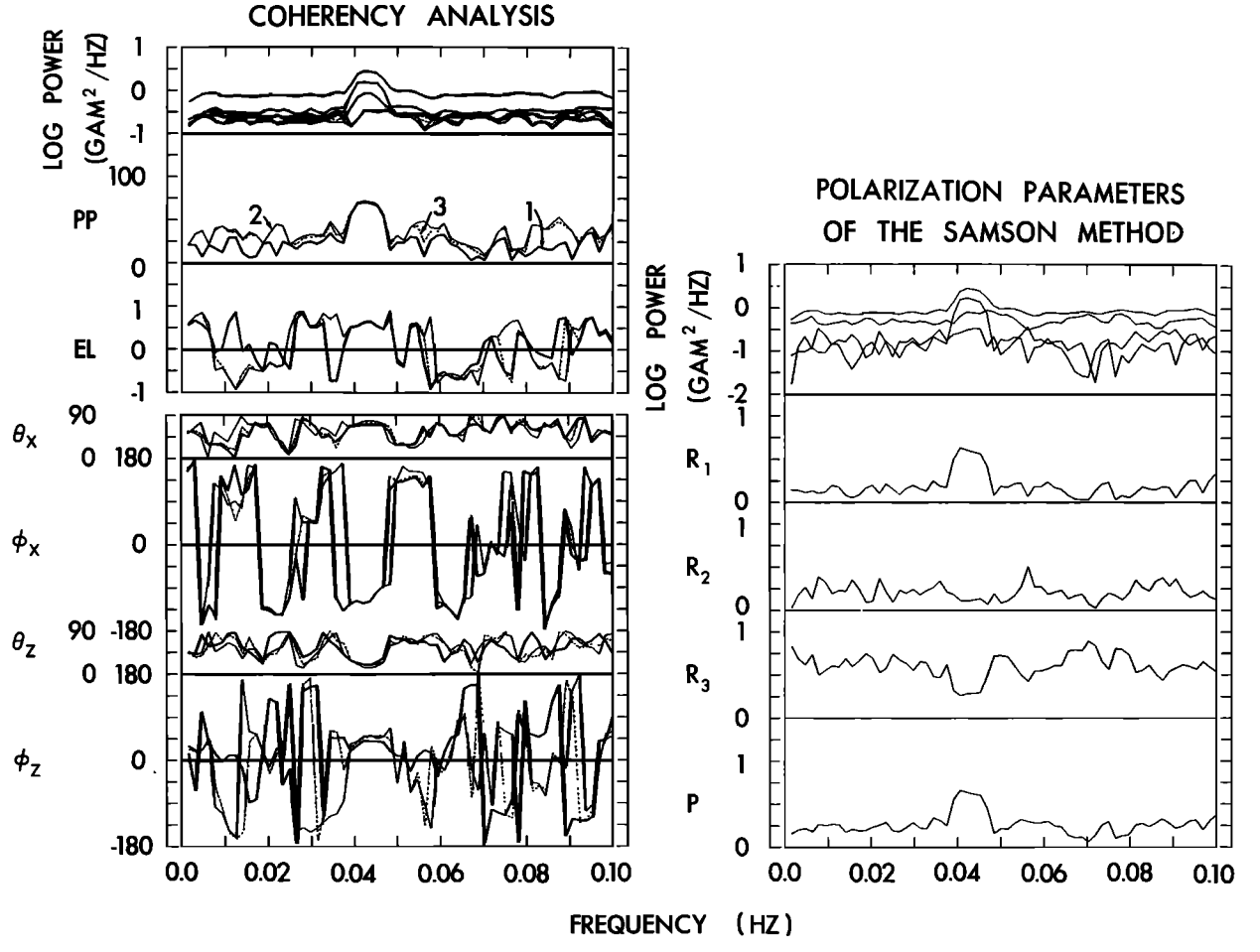

Fig. 9. Analysis results for the event shown in Figure 8. The format is the same as Figure 7.

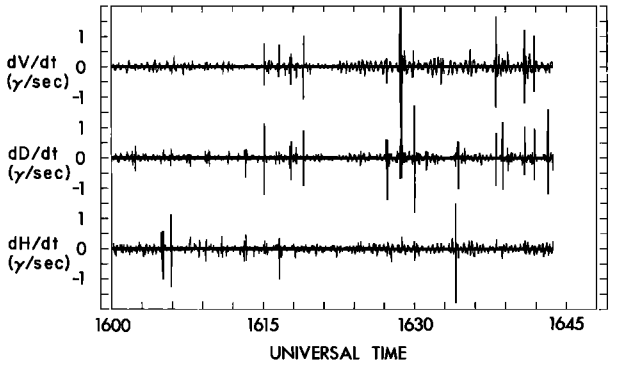

Fig. 10. Waveform of a Pc 3 event observed at ATS 1 on August 17, 1967, 1600–1643 UT. The data are first-differenced and in the dipole *VDH* system.

more nearly approximates a real wave event. The results of the analysis for this event are shown in Figure 9. Once again there is excellent agreement between techniques and with the input parameters. The amount of power in the peak is much lower because of the shorter duration of the waves and the smaller snr. Because of the broadening of the spectral peaks introduced by the gaussian amplitude envelope, the two periods are not clearly distinguishable. Also, there is no indication of the presence of significant partially polarized power in R_2. In fact, R_3 is consistently higher than R_2. Although P is not large even at the peak of the power, it clearly indicates the presence of a polarized wave. Even though this simulated event approximates a

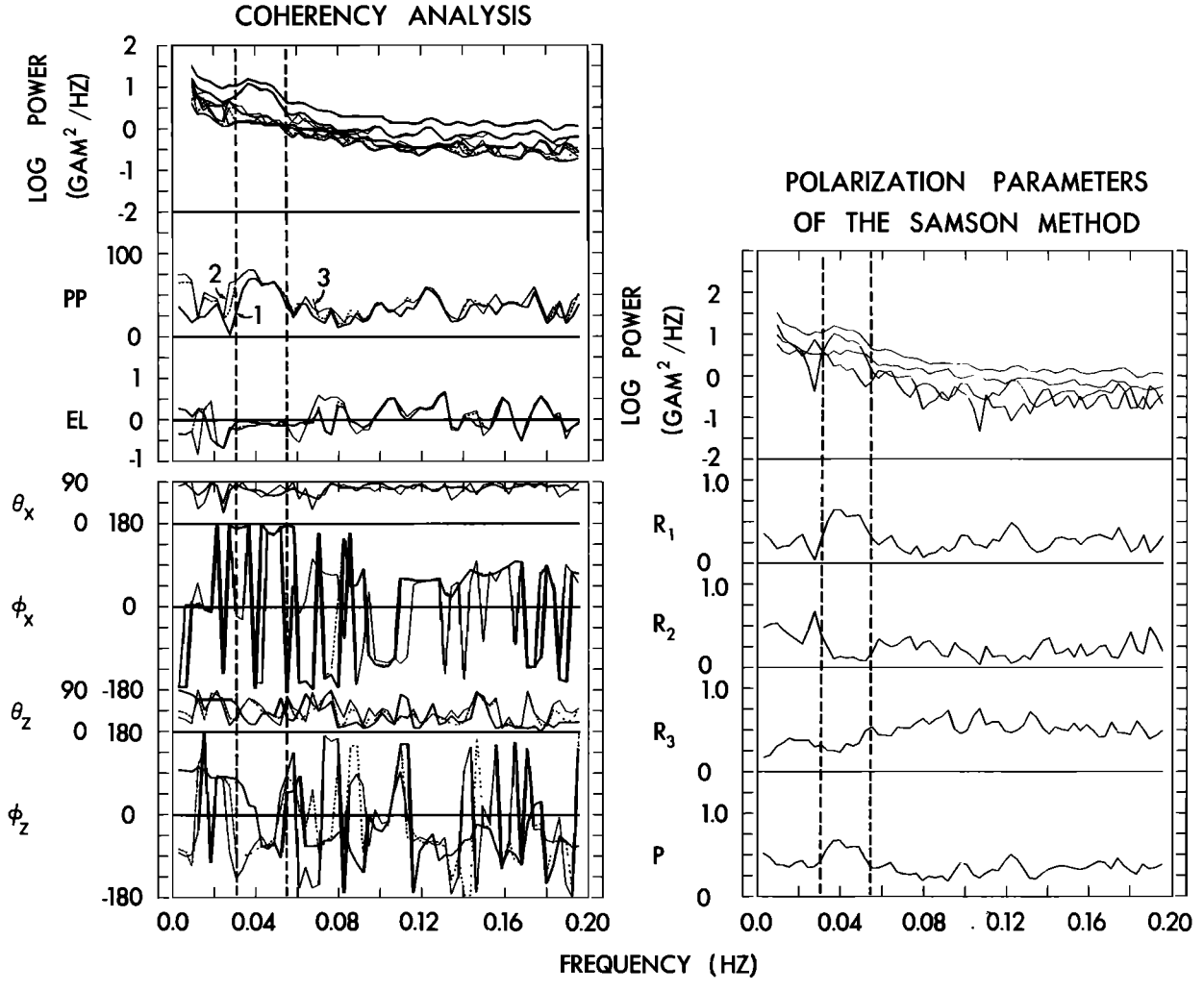

Fig. 11. Analysis results for the ATS 1 Pc 3 event shown in Figure 10. The format is the same as Figure 7, except that the vertical dashed lines indicate the boundaries of the band of wave activity.

real wave event, it is still much less complex than most real wave signals, so the performance of the three techniques on examples of real events must also be examined.

Real wave events. Two examples of Pc 3 micropulsations (quasisinusoidal magnetic variations in the 10-45 sec period range) were selected to test the performance of the three techniques on real wave events. One event was observed by the geosynchronous satellite ATS 1, which typically produces very noisy data. The *VDH* coordinate system in which both of these events are presented is the dipole *VDH* system: the $\hat{H}$ axis is parallel to the earth's dipole axis; $\hat{D}$ is azimuthally eastward and perpendicular to a plane defined by $\hat{H}$ and a radius vector through the spacecraft; and $\hat{V}$ completes the right-hand system such that $\hat{V} \times \hat{D} = \hat{H}$.

The waveform of the ATS 1 event is shown in Figure 10. The data are 2.56 sec averages which have been first-differenced, and most of the spikes have been removed. The spectrum is recolored to compensate for the prewhitening introduced by the first-differencing. The results obtained with the three techniques are shown in Figure 11. There is good agreement between the results of the three techniques for the band of interest, indicated by the dashed vertical lines. All three techniques indicate a highly polarized and very linear wave. Although the three techniques give somewhat different results for the orientation angles, the conclusions about the character of the waves are still basically the same: the wave is transverse with radial orientation, and its direction of propagation makes an angle of ~30° with $\hat{H}$. The results for the parameters of the *Samson* [1973] method are similar to those for the previous simulated event. Even though the spectral peak is not strong, the values of R_1 and P clearly indicate the presence of a polarized wave.

Because the data are so much quieter, nonderivative data are used in the analysis of the ATS 6 Pc 3 event illustrated in Figure 12. There are clearly frequencies besides that of Pc 3 present in this event. The long period oscillations in the V component are due to interference from another experiment on the spacecraft. The harmonics of this interference are clear in the spectrum shown in Figure 13. However, they do not obscure in any way the strong broad Pc 3 band indicated by the dashed lines. There is excellent agreement between the three techniques on all the characteristics of

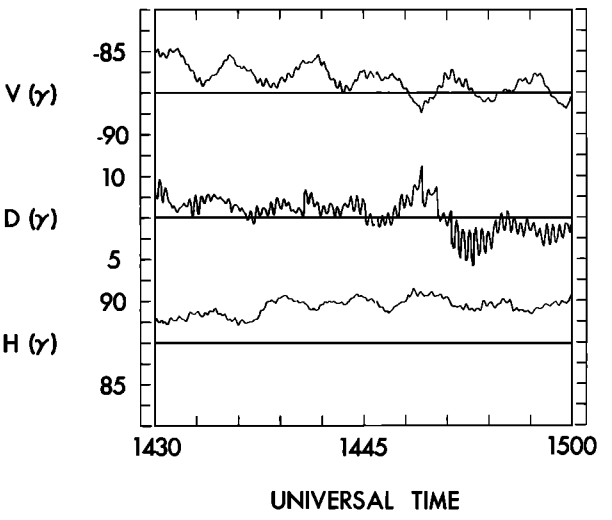

Fig. 12. Waveform of a portion of a Pc 3 event observed at ATS 6 on July 9, 1974, 1430-1500 UT. The data are given in the dipole *VDH* system.

this event. This wave is linear, highly polarized, azimuthal and transverse. The θ_z angle is ~30°. The complexity of the spectrum is evident in the *Samson* [1973] method parameters as well. However, the wave band is as clear here as before. Both R_1 and P are high across the band, and R_3 is low. It is clear that P and R_1 have the same pattern. It is also interesting to note that in general R_2 decreases when R_1 increases, and vice versa.

CONCLUSIONS

Performance. All three techniques performed equally well on the simulated wave events, giving excellent results down to quite low values of snr. All three analyzed simple simulated linear events equally well, and all three gave essentially the same results on the real wave events. The major performance difference was in the percent polarization determined for random noise. Because the 90% line fell at 30% polarization for technique 1 and at 40% for the other two techniques (see Figure 1), technique 1 should be slightly more useful in detecting weak wave signals in fairly noisy data.

Ease of coding. We mention ease of coding only as a minor point of comparison. It should not be considered a deciding factor between the techniques. Technique 1 is quite straightforward to code, particularly if eigenanalysis routines for real matrices are available. Technique 2 is slightly more

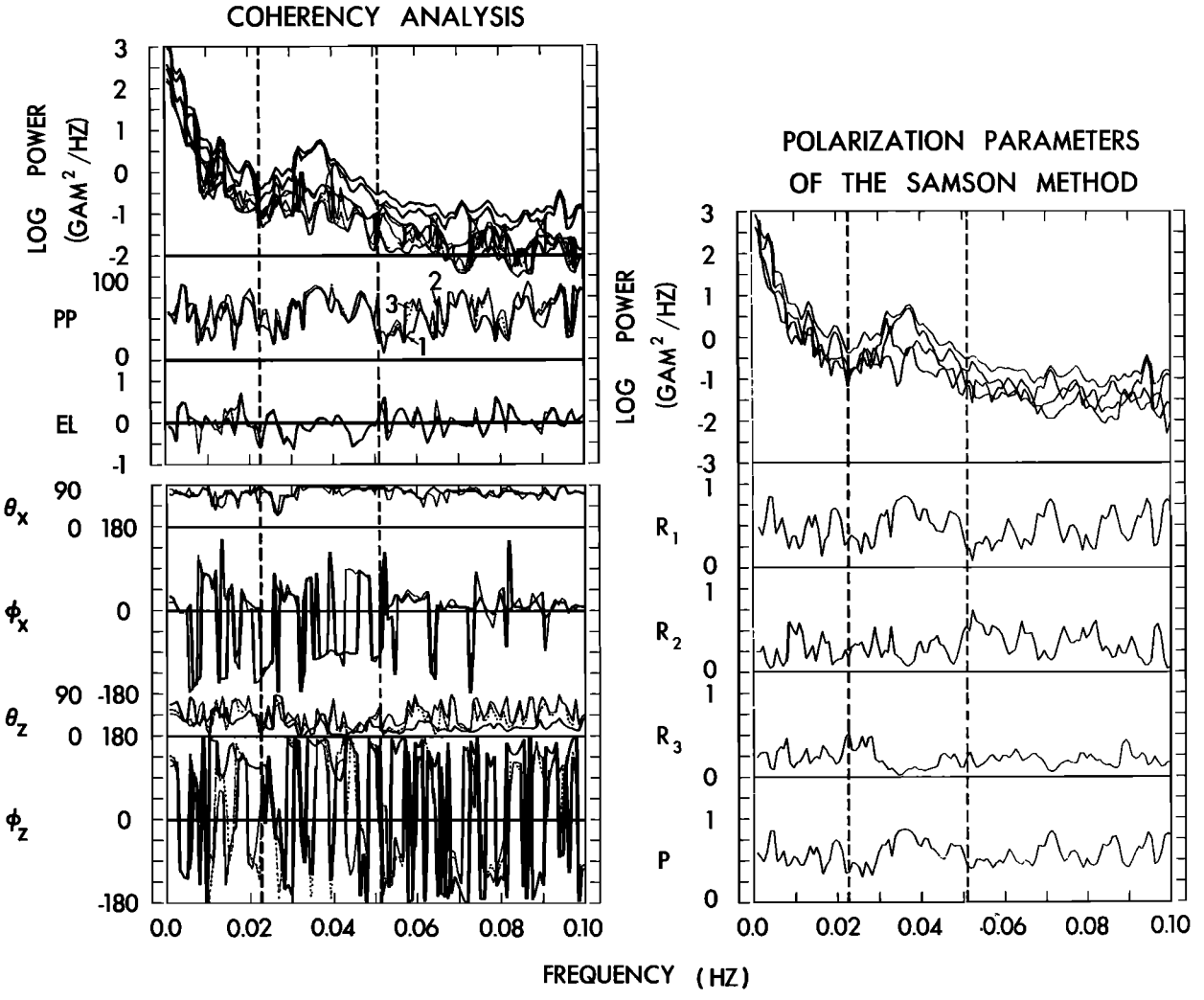

Fig. 13. Analysis results for the event illustrated in Figure 12. The format is the same as in Figure 11.

complicated to code and requires a slightly longer program. Technique 3 is organizationally quite complex to program. Without some programmed procedure such as EISPACK (or the algorithms from *Smith et al.* [1974]) for eigenanalysis of a complex matrix, coding of technique 3 is quite complex and difficult.

Cost effectiveness. To determine the relative cost effectiveness of the three techniques, comparisons were made of the cost of each to analyze the same data. Because technique 2 requires no eigenanalysis, it might be expected to be significantly cheaper than the other techniques. However, because of the larger number of computations required, it is only slightly less expensive than technique 1. Technique 3 is half again as expensive as either of the other two techniques. This is due partly to the complex eigenanalysis required and partly to the extra computations necessary to determine both sets of parameters. However, if a simpler method of extracting the physically meaningful parameters from the unitary matrix of eigenvectors can be found, this technique could be the most useful since it provides more parameters with which to characterize the waves. The differences in cost are not considerable enough to be an important factor in studies involving only a few events. However, in statistical studies involving large numbers of events and requiring wave analysis of hundreds of power spectra, the relative cost effec-

tiveness of the various techniques may be of significant importance.

Recommendations. None of the techniques is obviously superior to the others in terms of performance. However, in its present state of development, technique 3 is much less cost-effective than the other two, and thus is not as highly recommended for studies of large numbers of events. In choosing between techniques 1 and 2, the nature of the events may provide the best basis for selection. If the waves being studied are seldom linear, technique 2 is probably the best choice, although problems may arise if the data are very noisy because of the percent polarization found for random noise. For waves which are usually linear (such as Pc 3), technique 1 is probably the best. Although technique 2 did well on the simple test with linear waves, a much more thorough study of its performance for ellipticities < 0.1 in complicated events is necessary before it can be strongly recommended for use in the study of predominantly linear waves.

Acknowledgments. This work was supported in part by NASA grants NGL 05-007-004 and NAS 5-11674. We wish to thank N. Cline for his many helpful contributions.

REFERENCES

Born, J., and E. Wolf (1964), *Principles of Optics*, pp. 544-555, Macmillan, New York.

Fowler, R. A., B. J. Kotick, and R. D. Elliot (1967), Polarization analysis of naturally and artificially induced geomagnetic micropulsations, *J. Geophys. Res.*, *72*, 2871-2883.

McPherron, R. L., C. T. Russell, and P. J. Coleman, Jr. (1972), Fluctuating magnetic fields in the magnetosphere, 2, ULF waves, *Space Sci. Rev.*, *13*, 411-454.

Means, J. D. (1972), Use of the three-dimensional covariance matrix in analyzing the polarization properties of plane waves, *J. Geophys. Res.*, *77*, 5551-5559.

Samson, J. C. (1973), Descriptions of the polarization states of vector processes: Applications to ULF magnetic fields, *Geophys. J. Roy. Astron. Soc.*, *34*, 403-419.

Smith, B. T., J. M. Boyle, B. S. Garbow, Y. Ikebe, V. C. Klema, and C. B. Moler (1974), *Matrix Eigensystem Routines-EISPACK Guide*, 387 pp., Springer, New York.